

Unpaired Image-to-Image Translation via Neural Schrödinger Bridge

Beomsu Kim^{*1} Gihyun Kwon^{*2} Kwanyoung Kim¹ Jong Chul Ye¹

^{*}Equal contribution

¹Kim Jaechul Graduate School of AI, KAIST

²Department of Bio and Brain Engineering, KAIST

{beomsu.kim, cyclomon, cubeyoung, jong.ye}@kaist.ac.kr

Abstract

Diffusion models are a powerful class of generative models which simulate stochastic differential equations (SDEs) to generate data from noise. Although diffusion models have achieved remarkable progress in recent years, they have limitations in the unpaired image-to-image translation tasks due to the Gaussian prior assumption. Schrödinger Bridge (SB), which learns an SDE to translate between two arbitrary distributions, have risen as an attractive solution to this problem. However, none of SB models so far have been successful at unpaired translation between high-resolution images. In this work, we propose the Unpaired Neural Schrödinger Bridge (UNSB), which combines SB with adversarial training and regularization to learn a SB between unpaired data. We demonstrate that UNSB is scalable, and that it successfully solves various unpaired image-to-image translation tasks. Code: <https://github.com/cyclomon/UNSB>

1 Introduction

Diffusion models [1, 2, 3, 4], a class of generative model which generate data by simulating stochastic differential equations (SDEs), have achieved remarkable progress. They are capable of diverse and high-quality sample synthesis [5], a desiderata which was difficult to obtain for several widely acknowledged models such as Generative Adversarial Networks (GANs) [6], Variational Autoencoders (VAEs) [7], and flow-based models [8]. Furthermore, the iterative nature of diffusion models proved to be useful for a variety of applications, e.g., image restoration [9] and conditional generation [10].

However, unlike GANs which are free to choose any prior distribution, diffusion models often assume a simple prior, such as the Gaussian distribution. In other words, the initial condition for diffusion SDEs is generally fixed to be Gaussian noise. The Gaussian assumption prevents diffusion models from unlocking their full potential in unpaired image-to-image translation tasks such as domain transfer, style transfer, or unpaired image restoration.

Schrödinger bridges (SBs), a subset of SDEs, present a promising solution to this issue. They solve the entropy-regularized optimal transport (OT) problem, enabling translation between two arbitrary distributions. Their flexibility have motivated several approaches to solving SBs via deep learning. For instance, Bortoli et al. [11] extends the Iterative Proportional Fitting (IPF) procedure to the continuous setting, Chen et al. [12] proposes likelihood training of SBs using Forward-Backward SDEs theory, and Tong et al. [13] solves the SB problem with a conditional variant of flow matching.

Some methods have solved SBs assuming one side of the two distributions is simple. Wang et al. [14] developed a two-stage unsupervised procedure for estimating the SB between a Dirac delta and data. I²SB [15] and InDI [16] uses paired data to learn SBs between Dirac delta and data. Su et al. [17] discovered DDIMs [3] as SBs between data and Gaussian distributions. Hence, they were able

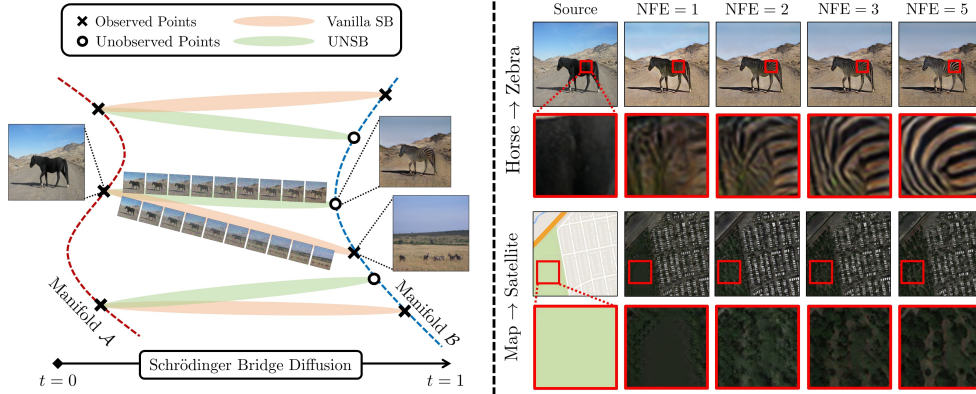


Figure 1: **Left:** Due to the curse of dimensionality, observed samples / training data in high dimensions become sparse and fail to describe image manifolds accurately. Vanilla SB learns optimal transport between observed samples, leading to undesirable mappings. UNSB employs adversarial learning and regularization to learn an optimal transport mapping which successfully generalizes beyond observed data. **Right:** UNSB can be interpreted as successively refining the predicted target domain image, enabling the model to modify fine details while preserving semantics. See Section 4.4. Here, NFE stands for the number of neural net function evaluations.

to perform image-to-image translation by concatenating two DDIMs, i.e., by passing through an intermediate Gaussian distribution.

Yet, to the best of our knowledge, no work so far has successfully trained SBs for direct translation between high-resolution images in the unpaired setting. Some methods demand excessive computation, and even if it is not the case, we observe poor results. In fact, none of OT-based methods considered in this work succeed in the simplest of unpaired data-to-data or image-to-image translation tasks.

In this work, we first identify the main culprit behind the failure of SB for unpaired image-to-image translation as the curse of dimensionality. As the dimension of the considered data increases, the samples become increasingly sparse, failing to capture the shape of the underlying image manifold. This sampling error then biases the SB optimal transport map, leading to an inaccurate SB.

We then propose the Unpaired Neural Schrödinger Bridge (UNSB), which tackles the curse of dimensionality through two components: adversarial learning, and regularization. Adversarial learning exploits the generalization ability of deep neural nets to learn a smooth representation of the data manifold. Regularization further enforces the SB to learn a mapping which aligns with our inductive bias. Furthermore, both components are scalable, so UNSB is naturally scalable as well.

Experiments on toy and practical image-to-image translation tasks demonstrate that UNSB indeed mitigates the curse of dimensionality. Hence, UNSB opens up a new research direction for applying diffusion models to unpaired translation tasks. Our contributions can be summarized as follows.

- We identify the cause behind the failure of previous SB methods for image-to-image translation as the curse of dimensionality. We propose a toy task which serves as a sanity check for whether an OT-based method is robust to the curse of dimensionality.
- We propose UNSB, which overcomes the curse of dimensionality through two components: adversarial learning and regularization. UNSB can be interpreted as improving upon the Denoising Diffusion GAN [5], by enabling translation between two arbitrary distributions.
- We demonstrate UNSB passes the sanity check, which provides evidence that it is resilient to the curse of dimensionality. Furthermore, UNSB is successful at a variety of image-to-image translation tasks, while previous OT methods fail.

2 Related Works

Schrödinger Bridges. The Schrödinger bridge (SB) problem, commonly referred to as the entropy-regularized Optimal Transport (OT) problem [18, 19], is the task of learning a stochastic process that

transitions from an initial probability distribution to a terminal distribution over time, while subject to a reference measure. It is closely connected to the field of stochastic control problems [20, 21]. Recently, the remarkable characteristic of the SB problem, which allows for the choice of arbitrary distributions as the initial and terminal distributions, has facilitated solutions to various generative modeling problems. In particular, novel algorithms leveraging Iterative Proportional Fitting (IPF) [11, 22] have been proposed to approximate score-based diffusion. Building upon these algorithms, several variants have been introduced and successfully applied in diverse fields such as, inverse problems [23], Mean field of Game [24], constrained transport problems [25], Riemannian manifolds [26], and path samplers [27, 28]. Some methods have solved SBs assuming one side of the two distributions is simple. In the unsupervised setting, Wang et al. [14] first learns a SB between a Dirac delta and noisy data, and then denoises the noisy samples. In the supervised setting, I²SB [15] and InDI [16] uses paired data to learn SBs between Dirac delta and data. DDIB [17] concatenates two SBs between data and the Gaussian distribution for image-to-image translation. However, to the best of our knowledge, the SB problem has not been previously investigated in the context of direct translation between unpaired images. Our work represents the first endeavor on this problem.

Unpaired image-to-image translation. The aim of image-to-image translation (I2I) is to produce an image in the target domain that preserves the structural similarity to the source image. A seminal work in I2I is pix2pix [29], which undertook the task with paired training images, utilizing a straightforward pixel-wise regularization strategy. However, this approach is not applicable when dealing with unpaired training settings. In the context of unpaired data settings, early methods like [30, 31] maintained the consistency between the source and output images through a two-sided training strategy, namely cycle-consistency. However, these models are plagued by inefficiencies in training due to the necessity of additional generator training. In order to circumvent this issue, recent I2I models have shifted their focus to one-sided I2I translation. They aim to preserve the correspondence between the input and output through various strategies, such as geometric consistency [32] and mutual information regularization [33]. Recently, Contrastive Unpaired Translation (CUT) and its variants [34, 35, 36, 37] have demonstrated improvements in I2I tasks by refining patch-wise regularization strategies. Despite the impressive performance demonstrated by previous GAN-based models in the I2I domain, we believe our SB-based approach paves the way for further improvements in the I2I task. It represents a new paradigm of potential in the ongoing advancement of image-to-image translation.

3 Schrödinger Bridges and the Curse of Dimensionality

Given two distributions π_0, π_1 on \mathbb{R}^d , the Schrödinger Bridge problem (SBP) seeks the most likely random process $\{\mathbf{x}_t : t \in [0, 1]\}$ that interpolates π_0 and π_1 . Specifically, let Ω be the path space on \mathbb{R}^d , i.e., the space of continuous functions from $[0, 1]$ to \mathbb{R}^d , and let $\mathcal{P}(\Omega)$ be the space of probability measures on Ω . Then, the SBP solves

$$\mathbb{Q}^{\text{SB}} = \arg \min_{\mathbb{Q} \in \mathcal{P}(\Omega)} D_{\text{KL}}(\mathbb{Q} \parallel \mathbb{W}^\tau) \quad \text{s.t.} \quad \mathbb{Q}_0 = \pi_0, \quad \mathbb{Q}_1 = \pi_1 \quad (1)$$

where \mathbb{W}^τ is the Wiener measure with variance τ , and \mathbb{Q}_t denotes the marginal of \mathbb{Q} at time t . We call \mathbb{Q}^{SB} the Schrödinger Bridge (SB) between π_0 and π_1 .

The SBP admits multiple alternative formulations, and among those, the stochastic control formulation and the conditional flow matching (CFM) formulation play crucial roles in our work. Specifically, both formulations will serve as theoretical bases for our Unpaired Neural Schrödinger Bridge algorithm, and the CFM formulation will shed light on why previous SB methods have failed on unpaired image-to-image translation tasks.

Stochastic control formulation. The stochastic control formulation [38] shows that $\{\mathbf{x}_t\} \sim \mathbb{Q}^{\text{SB}}$ can be described by an Itô SDE

$$d\mathbf{x}_t = \mathbf{u}_t^{\text{SB}} dt + \sqrt{\tau} d\mathbf{w}_t \quad (2)$$

where the time-varying drift \mathbf{u}_t^{SB} is a solution to the stochastic control problem

$$\mathbf{u}_t^{\text{SB}} = \arg \min_{\mathbf{u}} \mathbb{E} \left[\int_0^1 \frac{1}{2} \|\mathbf{u}_t\|^2 dt \right] \quad \text{s.t.} \quad \begin{cases} d\mathbf{x}_t = \mathbf{u}_t dt + \sqrt{\tau} d\mathbf{w}_t \\ \mathbf{x}_0 \sim \pi_0, \quad \mathbf{x}_1 \sim \pi_1 \end{cases} \quad (3)$$

assuming \mathbf{u} satisfies certain regularity conditions. Eq. (3) says that among the SDEs of the form Eq. (2) with boundaries π_0 and π_1 , the drift for the SDE describing the SB has minimum energy.

This formulation also reveals two useful properties of SBs. First, $\{\mathbf{x}_t\}$ is a Markov chain, and second, $\{\mathbf{x}_t\}$ converges to the optimal transport ODE trajectory as $\tau \rightarrow 0$. Intuitively, τ controls the amount of randomness in the trajectory $\{\mathbf{x}_t\}$.

CFM formulation. The CFM formulation [13] of SBP shows that sampling from \mathbb{Q}^{SB} is extremely simple, assuming we know the joint distribution of the SB at $t \in \{0, 1\}$, denoted as $\mathbb{Q}_{01}^{\text{SB}}$. Concretely, for $\{\mathbf{x}_t\} \sim \mathbb{Q}^{\text{SB}}$, conditioned upon initial and terminal points \mathbf{x}_0 and \mathbf{x}_1 , the density of \mathbf{x}_t can be described by a Gaussian density

$$p(\mathbf{x}_t | \mathbf{x}_0, \mathbf{x}_1) = \mathcal{N}(\mathbf{x}_t | t\mathbf{x}_1 + (1-t)\mathbf{x}_0, t(1-t)\tau\mathbf{I}). \quad (4)$$

Hence, to simulate the SB given an initial point \mathbf{x}_0 , we may sample \mathbf{x}_t according to

$$p(\mathbf{x}_t | \mathbf{x}_0) = \int p(\mathbf{x}_t | \mathbf{x}_0, \mathbf{x}_1) d\mathbb{Q}_{1|0}^{\text{SB}}(\mathbf{x}_1 | \mathbf{x}_0) \quad (5)$$

where $\mathbb{Q}_{1|0}^{\text{SB}}$ denotes the conditional distribution of \mathbf{x}_1 given \mathbf{x}_0 .

Surprisingly, $\mathbb{Q}_{01}^{\text{SB}}$ is shown to be a solution to the entropy-regularized optimal transport problem

$$\mathbb{Q}_{01}^{\text{SB}} = \arg \min_{\gamma \in \Pi(\pi_0, \pi_1)} \mathbb{E}_{(\mathbf{x}_0, \mathbf{x}_1) \sim \gamma} [\|\mathbf{x}_0 - \mathbf{x}_1\|^2] - 2\tau H(\gamma) \quad (6)$$

where $\Pi(\pi_0, \pi_1)$ is the collection of joint distributions whose marginals are π_0 and π_1 , and H denotes the entropy function. For discrete π_0 and π_1 , it is possible to find $\mathbb{Q}_{01}^{\text{SB}}$ via the Sinkhorn-Knopp algorithm, and this observation has inspired several algorithms [13, 39] for approximating the SB.

3.1 Curse of Dimensionality

According to the CFM formulation of the SBP, any algorithm for solving the SBP can be interpreted as learning an interpolation according to the entropy-regularized optimal transport Eq. (6) of the marginals π_0 and π_1 . However, in practice, we only have a finite number of samples $\{\mathbf{x}_0^n\}_{n=1}^N \sim \pi_0$ and $\{\mathbf{x}_1^m\}_{m=1}^M \sim \pi_1$. This means, the SB is trained to transport samples between the empirical distributions $\frac{1}{N} \sum_{n=1}^N \delta_{\mathbf{x}_0^n}$ and $\frac{1}{M} \sum_{m=1}^M \delta_{\mathbf{x}_1^m}$. Due to the curse of dimensionality, the samples fail to describe the image manifolds correctly in high dimension. Ultimately, $\mathbb{Q}_{01}^{\text{SB}}$ yield image pairs that do not meaningfully correspond to one another (see Figure 1 or the result for Neural Optimal Transport (NOT) in Figure 5).

To illustrate this phenomenon in the simplest scenario, we consider the case where π_0 and π_1 are supported uniformly on two concentric d -spheres of radii 1 and 2, respectively. Then, samples from $\mathbb{Q}_{01}^{\text{SB}}$ should have near-one cosine similarity, since \mathbb{Q}^{SB} should transport samples from π_0 radially outwards. However, when we draw $M = N = 1000$ i.i.d. samples from π_0 and π_1 , and calculate the cosine similarity between $(\mathbf{x}_0, \mathbf{x}_1) \sim \mathbb{Q}_{01}^{\text{SB}}$ where $\mathbb{Q}_{01}^{\text{SB}}$ is estimated using the Sinkhorn-Knopp algorithm, we observe decreasing similarity as dimension increases (see Figure 2). Thus, in a high dimension, \mathbb{Q}^{SB} approximated by Sinkhorn-Knopp will interpolate between nearly orthogonal points. In the next section, we propose the Unpaired Neural Schrödinger Bridge to combat the curse of dimensionality.

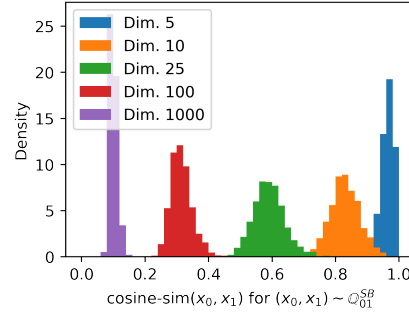


Figure 2: Curse of dimensionality.

4 Unpaired Neural Schrödinger Bridge (UNSB)

In practice, we simulate a discretization of $\{\mathbf{x}_t\} \sim \mathbb{Q}^{\text{SB}}$. Specifically, given a partition $\{t_i\}_{i=0}^N$ of the unit interval $[0, 1]$ such that $t_0 = 0$, $t_N = 1$, and $t_i < t_{i+1}$, we can simulate SB according to the Markov chain decomposition

$$p(\{\mathbf{x}_{t_n}\}) = p(\mathbf{x}_{t_N} | \mathbf{x}_{t_{N-1}}) p(\mathbf{x}_{t_{N-1}} | \mathbf{x}_{t_{N-2}}) \cdots p(\mathbf{x}_{t_1} | \mathbf{x}_{t_0}) p(\mathbf{x}_{t_0}). \quad (7)$$

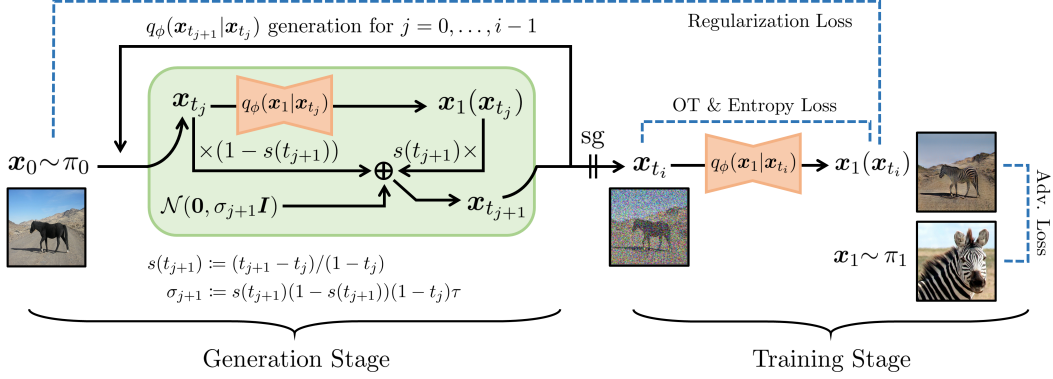


Figure 3: Generation and training process of UNSB for time step t_i . sg means stop gradient.

Since the distribution of $\mathbf{x}_{t_0} = \mathbf{x}_0$ is already known as π_0 , our main interest lies in learning the transition probabilities $p(\mathbf{x}_{t_{i+1}}|\mathbf{x}_{t_i})$ for $i = 0, \dots, N-1$.

The decomposition Eq. (7) allows us to learn the SB inductively, i.e., we learn $p(\mathbf{x}_{t_{i+1}}|\mathbf{x}_{t_i})$ assuming we are able to sample from $p(\mathbf{x}_{t_i})$. The construction proceeds in two steps. First, we show that the SB satisfies a certain self-similarity property, which states that the SB restricted any sub-interval of $[0, 1]$ is also a SB. Next, we use self-similarity to show that $p(\mathbf{x}_{t_{i+1}}|\mathbf{x}_{t_i})$ can be found by solving an adversarial learning objective with identity and entropy regularizations.

4.1 Self-similarity of SBs

Theorem 1, proved using Eq. (3), tells us that a SB restricted to a sub-interval of $[0, 1]$ also solves the SBP. One notable difference from the original SBP Eq. (1) is that the reference Wiener process has reduced variance $\tau(t_b - t_a)$. Intuitively, this is because we are dealing with a smaller interval, so we have less randomness in the SB. While Theorem 1 is rather abstract, its CFM formulation in Corollary 1.1 provides us with concrete formulas for simulating restricted SBs. Thus, Corollary 1.1 will serve as a foundation for learning $p(\mathbf{x}_{t_{i+1}}|\mathbf{x}_{t_i})$ for $i = 0, \dots, N-1$ in Eq. (7).

Theorem 1 (Self-similarity). *Let $[t_a, t_b] \subseteq [0, 1]$ and $\{\mathbf{x}_t\} \sim \mathbb{Q}^{\text{SB}}$. The SB restricted to $[t_a, t_b]$, defined as the distribution of $\{\mathbf{x}_t\}_{|[t_a, t_b]} := \{\mathbf{x}_{t(s)} : s \in [0, 1]\}$ where $t(s) := t_a + (t_b - t_a)s$ solves*

$$\min_{\mathbb{Q} \in \mathcal{P}(\Omega)} D_{\text{KL}}(\mathbb{Q} \| \mathbb{W}^{\tau(t_b - t_a)}) \quad \text{s.t.} \quad \mathbb{Q}_0 = \mathbb{Q}_{t_a}^{\text{SB}}, \quad \mathbb{Q}_1 = \mathbb{Q}_{t_b}^{\text{SB}}. \quad (8)$$

Corollary 1.1 (CFM formulation of restricted SBs). *Let $t \in [t_a, t_b] \subseteq [0, 1]$ and $\{\mathbf{x}_t\} \sim \mathbb{Q}^{\text{SB}}$. Then*

$$p(\mathbf{x}_t|\mathbf{x}_{t_a}, \mathbf{x}_{t_b}) = \mathcal{N}(\mathbf{x}_t | s(t)\mathbf{x}_{t_b} + (1 - s(t))\mathbf{x}_{t_a}, s(t)(1 - s(t))\tau(t_b - t_a)\mathbf{I}) \quad (9)$$

where $s(t) := (t - t_a)/(t_b - t_a)$ is the inverse function of $t(s)$. Moreover,

$$\mathbb{Q}_{t_a t_b}^{\text{SB}} = \arg \min_{\gamma \in \Pi(\mathbb{Q}_{t_a}, \mathbb{Q}_{t_b})} \mathbb{E}_{(\mathbf{x}_{t_a}, \mathbf{x}_{t_b}) \sim \gamma} [\|\mathbf{x}_{t_a} - \mathbf{x}_{t_b}\|^2] - 2\tau(t_b - t_a)H(\gamma). \quad (10)$$

4.2 Lagrangian Formulation

As noted in the previous section, we now use Corollary 1.1 to learn $p(\mathbf{x}_{t_{i+1}}|\mathbf{x}_{t_i})$ in Eq. (7) assuming we can sample from $p(\mathbf{x}_{t_i})$. Let $q_{\phi_i}(\mathbf{x}_1|\mathbf{x}_{t_i})$ be a conditional distribution parametrized by a DNN with parameter ϕ_i . Intuitively, $q_{\phi_i}(\mathbf{x}_1|\mathbf{x}_{t_i})$ predicts the target domain image for \mathbf{x}_{t_i} . We define

$$q_{\phi_i}(\mathbf{x}_{t_i}, \mathbf{x}_1) := q_{\phi_i}(\mathbf{x}_1|\mathbf{x}_{t_i})p(\mathbf{x}_{t_i}), \quad q_{\phi_i}(\mathbf{x}_1) := \mathbb{E}_{p(\mathbf{x}_{t_i})}[q_{\phi_i}(\mathbf{x}_1|\mathbf{x}_{t_i})]. \quad (11)$$

With Eq. (11) and Eq. (9), we also define

$$q_{\phi_i}(\mathbf{x}_{t_{i+1}}|\mathbf{x}_{t_i}) := \mathbb{E}_{q_{\phi_i}(\mathbf{x}_1|\mathbf{x}_{t_i})}[p(\mathbf{x}_{t_{i+1}}|\mathbf{x}_1, \mathbf{x}_{t_i})], \quad q_{\phi_i}(\mathbf{x}_{t_{i+1}}) := \mathbb{E}_{p(\mathbf{x}_{t_i})}[q_{\phi_i}(\mathbf{x}_{t_{i+1}}|\mathbf{x}_{t_i})]. \quad (12)$$

We then note the optimization problem Eq. (10) with $t_a = t_i$ and $t_b = 1$ may be expressed as

$$\begin{aligned} \min_{\phi_i} \quad & \mathcal{L}_{\text{SB}}(\phi_i, t_i) := \mathbb{E}_{q_{\phi_i}(\mathbf{x}_1|\mathbf{x}_{t_i})p(\mathbf{x}_{t_i})} [\|\mathbf{x}_{t_i} - \mathbf{x}_1\|^2] - 2\tau(1 - t_i)H(q_{\phi_i}(\mathbf{x}_{t_i}, \mathbf{x}_1)) \\ \text{s.t.} \quad & \mathcal{L}_{\text{Adv}}(\phi_i, t_i) := D_{\text{KL}}(q_{\phi_i}(\mathbf{x}_1) \| p(\mathbf{x}_1)) = 0. \end{aligned} \quad (13)$$

By incorporating the equality constraint into the loss with a Lagrange multiplier, we obtain the UNSB objective for a single time-step t_i

$$\min_{\phi_i} \mathcal{L}_{\text{UNSB}}(\phi_i, t_i) := \mathcal{L}_{\text{Adv}}(\phi_i, t_i) + \lambda_{\text{SB}, t_i} \mathcal{L}_{\text{SB}}(\phi_i, t_i). \quad (14)$$

Having solved Eq. (14) to approximate $p(\mathbf{x}_1 | \mathbf{x}_{t_i})$ by $q_{\phi_i}(\mathbf{x}_1 | \mathbf{x}_{t_i})$, we can use Eq. (12) to simulate $p(\mathbf{x}_{t_{i+1}} | \mathbf{x}_{t_i})$ and $p(\mathbf{x}_{i+1})$ via $q_{\phi_i}(\mathbf{x}_{t_{i+1}} | \mathbf{x}_{t_i})$ and $q_{\phi_i}(\mathbf{x}_{t_{i+1}})$, allowing us to learn $p(\mathbf{x}_{i+2} | \mathbf{x}_{i+1})$.

However, it is impractical to use separate parameters ϕ_i for each time-step t_i and to learn $p(\mathbf{x}_{t_{i+1}} | \mathbf{x}_{t_i})$ sequentially for $i = 0, \dots, N - 1$. Hence, in practice, we replace $q_{\phi_i}(\mathbf{x}_1 | \mathbf{x}_{t_i})$, which takes \mathbf{x}_{t_i} as input, with a time-conditional DNN $q_{\phi}(\mathbf{x}_1 | \mathbf{x}_{t_i})$, which shares a parameter ϕ for all time-steps t_i , and takes the tuple (\mathbf{x}_{t_i}, t_i) as input. Then, we optimize the sum of $\mathcal{L}_{\text{UNSB}}(\phi, t_i)$ over $i = 0, \dots, N - 1$.

4.3 Combating the Curse of Dimensionality

Adversarial learning. In practice, we can replace \mathcal{L}_{Adv} in Eq. (14) by any divergence or metric which measures discrepancy between two distributions. Such divergence or metric can be estimated through adversarial learning. This allows us to use various adversarial learning techniques to mitigate the curse of dimensionality. For instance, instead of discriminating generated and real samples on the instance level, we use a Markovian discriminator [29] to distinguish the samples on the patch level.

Regularization. Adversarial learning by itself may not be enough to overcome the curse of dimensionality. Hence, we augment the UNSB objective with regularization, which enforces the generator network q_{ϕ} to satisfy some notion of consistency between predicted \mathbf{x}_1 and the initial point \mathbf{x}_0 .

$$\mathcal{L}_{\text{Reg}}(\phi, t_i) := \mathbb{E}_{p(\mathbf{x}_0, \mathbf{x}_{t_i})} \mathbb{E}_{q_{\phi}(\mathbf{x}_1 | \mathbf{x}_{t_i})} [\mathcal{R}(\mathbf{x}_0, \mathbf{x}_1)] \quad (15)$$

Here, \mathcal{R} is a scalar-valued differentiable function which quantifies an application-specific measure of similarity between its inputs. In other words, \mathcal{R} reflects our inductive bias for similarity between two images. Thus, the UNSB objective for time t_i , in its final form, is

$$\mathcal{L}_{\text{UNSB}}(\phi, t_i) := \mathcal{L}_{\text{Adv}}(\phi, t_i) + \lambda_{\text{SB}, t_i} \mathcal{L}_{\text{SB}}(\phi, t_i) + \lambda_{\text{Reg}, t_i} \mathcal{L}_{\text{Reg}}(\phi, t_i). \quad (16)$$

4.4 Generation and Training

Generation. To simulate the SB using q_{ϕ} , we first sample $\mathbf{x}_0 \sim \pi_0$. Given \mathbf{x}_{t_j} (note that if $j = 0$, then $\mathbf{x}_{t_j} = \mathbf{x}_0$), we predict the target domain image $\mathbf{x}_1(\mathbf{x}_{t_j}) \sim q_{\phi}(\mathbf{x}_1 | \mathbf{x}_{t_j})$. By interpolating \mathbf{x}_0 and $\mathbf{x}_1(\mathbf{x}_{t_j})$ via Eq. (9) with $t_a = t_j$, $t_b = 1$, and $t = t_{j+1}$, we obtain $\mathbf{x}_{t_{j+1}}$. Repeating this procedure for $j = 0 \dots, i - 1$, we get \mathbf{x}_{t_i} . Thus, the trajectory $\{\mathbf{x}_1(\mathbf{x}_{t_i}) : i = 0, \dots, N - 1\}$ can be viewed as an iterative improvement of the predicted target domain sample. See the generation stage of Figure 3.

Training. We first randomly choose a time-step t_i to optimize. To calculate $\mathcal{L}_{\text{UNSB}}(\phi, t_i)$, we sample \mathbf{x}_{t_i} and $\mathbf{x}_1 \sim \pi_1$. \mathbf{x}_{t_i} is then passed through $q_{\phi}(\mathbf{x}_1 | \mathbf{x}_{t_i})$ to obtain $\mathbf{x}_1(\mathbf{x}_{t_i})$. The pair $(\mathbf{x}_{t_i}, \mathbf{x}_1(\mathbf{x}_{t_i}))$ is used to compute $\mathcal{L}_{\text{SB}}(\phi, t_i)$, $(\mathbf{x}_1, \mathbf{x}_1(\mathbf{x}_{t_i}))$ is used to calculate $\mathcal{L}_{\text{Adv}}(\phi, t_i)$, and $(\mathbf{x}_0, \mathbf{x}_1(\mathbf{x}_{t_i}))$ is used to calculate $\mathcal{L}_{\text{Reg}}(\phi, t_i)$. This process is illustrated in the training stage of Figure 3.

5 Experiments

5.1 Sanity Check on Toy Data

We show that with an appropriate regularization and adversarial training technique, UNSB can overcome the curse of dimensionality on the toy data of Section 3.1: we train the discriminator to distinguish real and fake samples by input norms, and choose negative cosine similarity as \mathcal{R} in Eq. (15). Only $1k$ samples from each π_0, π_1 are used throughout the training. In Figure 4, we compare Sinkhorn-Knopp (SK) and UNSB. We see $\mathbf{x}_1 \sim \mathbb{Q}_1^{\text{SB}}$ for \mathbb{Q}^{SB} found by both SK and UNSB have norm 2, so the samples lie on the target data manifold. However, when we compare the cosine similarity between \mathbf{x}_0 and \mathbf{x}_1 for $(\mathbf{x}_0, \mathbf{x}_1) \sim \mathbb{Q}_{01}^{\text{SB}}$, we find similarity decays for SK while UNSB is robust to dimension.

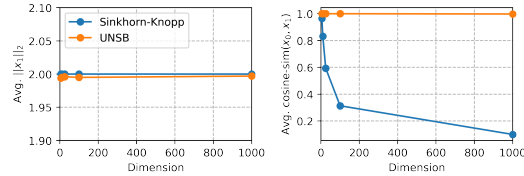


Figure 4: UNSB can mitigate the curse of dim.

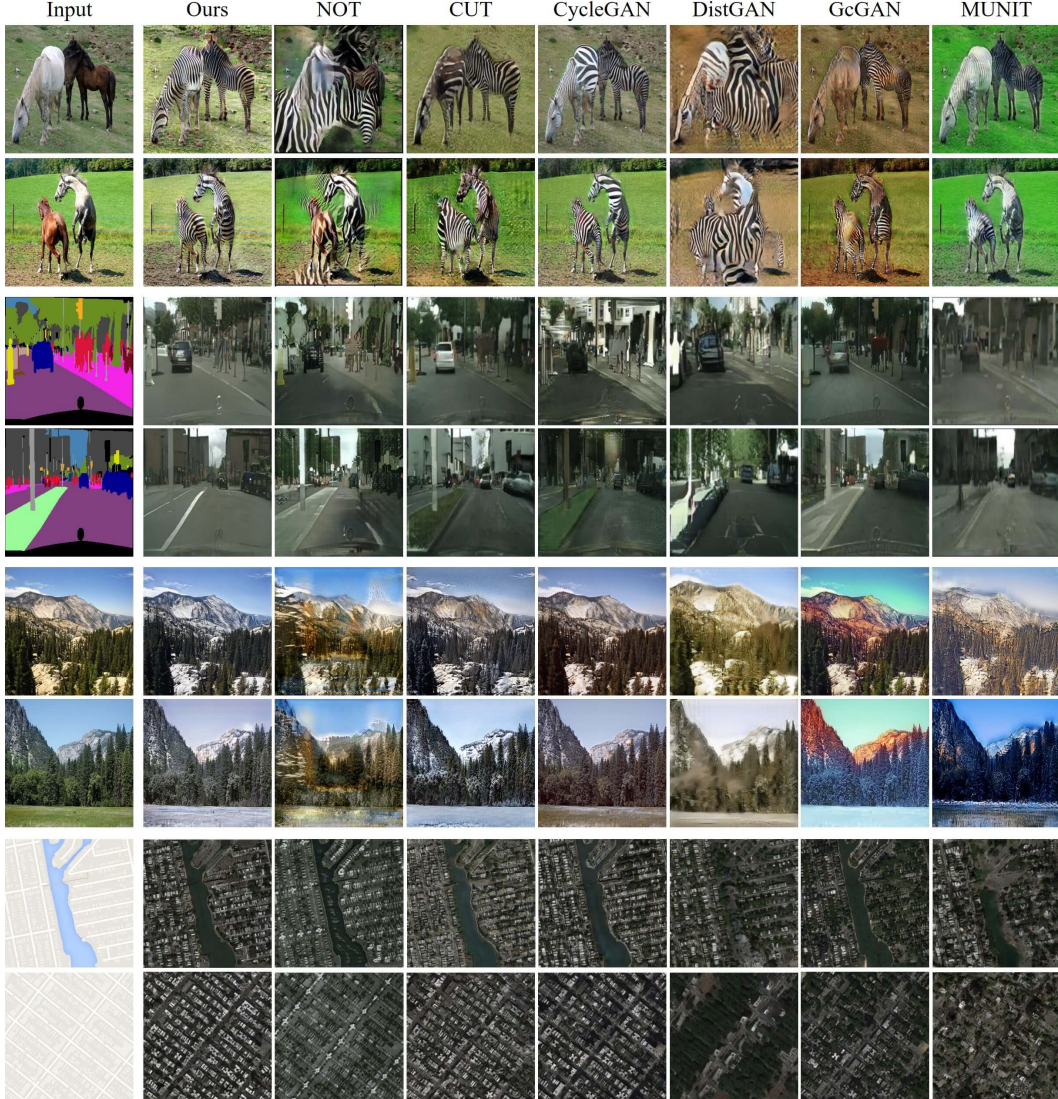


Figure 5: Qualitative comparison of image-to-image translation results from our UNSB and baseline I2I methods. Compared to other one-step baseline methods, our model generates more realistic domain-changed outputs while preserving the structural information of the source images.

5.2 Unpaired Image-to-Image Translation

Implementation details. Since our proposed method solves the curse of dimensionality problem, we can easily extend our method into high-resolution real image translation tasks.

For implementation, we referenced PyTorch implementation of recent unpaired image translation model of CUT [34]. For regularization loss \mathcal{L}_{Reg} , we leveraged the patch-wise contrastive matching scheme proposed in CUT. We set the number of timesteps as $N = 5$ so we discretize the unit interval into t_0, t_1, \dots, t_5 . To evaluate our proposed unpaired image translation model, we show the comparison results using various benchmark datasets: Horse \rightarrow Zebra, Map \rightarrow Cityscapes, Summer \rightarrow Winter, and Map \rightarrow Satellite images. All images are resized into 256×256 . For all the datasets, we trained the model for 400 epochs, with batch size of 1. We measure sample quality of $\mathbf{x}_1(\mathbf{x}_{t_i})$ for each $i = 0, \dots, N - 1$. So, NFE = i denotes sample evaluation or visualization of $\mathbf{x}_1(\mathbf{x}_{t_{i-1}})$. More details are elaborated in the Appendix.

Comparison results. To quantitatively evaluate our proposed model, we compared FID score [41] and KID score [42] obtained from baseline methods. For the baselines, we selected various GAN-

Method	Horse→Zebra		Label→Cityscape		Summer→Winter		Map→Satellite	
	FID↓	KID↓	FID↓	KID↓	FID↓	KID↓	FID↓	KID↓
CycleGAN[30]	77.2	1.957	76.3	3.532	84.9	1.022	54.6	3.430
MUNIT[31]	133.8	3.790	91.4	6.401	115.4	4.901	181.7	12.03
NOT[40]	104.3	5.012	221.3	19.76	185.5	8.732	224.9	16.59
Distance[33]	72.0	1.856	81.8	4.410	97.2	2.843	98.1	5.789
GcGAN[32]	86.7	2.051	105.2	6.824	97.5	2.755	79.4	5.153
CUT[34]	45.5	0.541	56.4	1.611	84.3	1.207	56.1	3.301
Ours-best	35.7	0.587	53.2	1.191	73.9	0.421	47.6	2.013

Table 1: Comparison results with FID and KID×100. Our model outperforms the baselines.

	H→Z	L→C	S→W	M→S
NFE = 1	53.4	74.3	75.2	71.3
NFE = 2	43.3	56.6	74.3	49.4
NFE = 3	38.5	53.5	74.2	47.6
NFE = 4	36.3	53.2	73.9	48.3
NFE = 5	35.7	54.8	74.9	52.0

Table 2: Quantitative ablation results. To verify the effect our SB-based image translation with respect to used NFEs, we show the FID scores calculated with generated images by varying the NFEs. H→Z: Horse→Zebra, L→C: Label→Cityscapes, S→W: Summer→Winter, M→S : Map→Satellite.

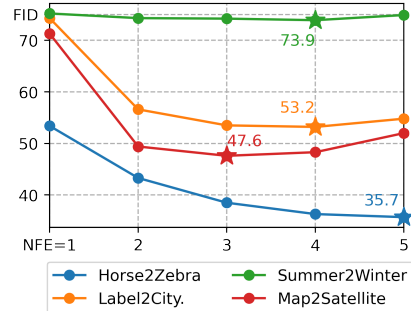


Figure 6: Visualization of FID score trending with respect to the number of NFEs used. Best results are starred.

based image translation models such as CycleGAN, MUNIT, DistanceGAN, GCGAN, and CUT. As an additional baseline, we used Neural Optimal Transport (NOT) [25] algorithm to represent OT-based I2I translation methods. Although there are several other SB or OT-based I2I translation methods, we did not include them in the main paper as the models do not scale well to high-resolution data. We show their results in the Appendix.

We show quantitative results in Table 1, where we observe our model outperforms baseline methods in all datasets. In particular, our model largely outperformed early GAN-based I2I baseline methods. When compared to recent models such as CUT, our model still shows better quantitative score. The OT-based method NOT suffers from degraded performance in all of the datasets. Importantly, $N = 1$ version of UNSB is nearly equivalent to CUT. So, we do see there is merit to choosing $N > 1$.

Qualitative comparison in Figure 5 provides insight into the superior performance of UNSB. Our model successfully translates source images to the target domain while preventing structural inconsistency. For other GAN-based methods, the model outputs do not properly reflect the target domain information, and some models fail to preserve source image structure. For NOT, we observe that the model failed to overcome the curse of dimensionality. Specifically, NOT hallucinates structures not present in the source image (for instance, see the first row of Figure 5), leading to poor samples.

5.3 Ablation Study

In order to analyze our UNSB algorithm, which allows multi-step translation of images, we conducted an ablation study to investigate the relationship between the number of function evaluations (NFE) in the inference step and the output sample quality.

First, we measured quantitative metrics by varying the NFE. From the results in Table 2 and Figure 6, we observed that using $NFE = 1$ resulted in relatively poor performance in all cases, sometimes even worse than existing one-step GAN methods. However, we found that increasing the NFE consistently improved generation quality. We observed that the best FIDs were achieved for NFE values between 3 and 5 for all datasets. Particularly noteworthy is that the Summer2Winter dataset exhibited good performance even for $NFE = 1$. We speculate that this is due to the lower difficulty of the I2I task on this dataset, allowing for good performance with a single step.



Figure 7: Qualitative ablation results for UNSB. Sample quality gradually improves with more NFEs.

This trend is also evident in our qualitative comparisons. Looking at Figure 7 which visualizes $x_1(x_{t_i})$ for $i = 0, \dots, 4$, when $\text{NFE} = 1$, the resulting images exhibit artifacts or color saturation. However, as NFE increases, there are gradual improvements in image quality. One exception is Summer2Winter, where UNSB already generates convincing Winter samples at $\text{NFE} = 1$.

6 Limitations, Societal Impacts, and Reproducibility

Limitations. UNSB at times suffers from the problem of “over-translation”, where the target domain style is excessively applied to the source image. We plan to investigate and address the source of this problem. We also note using high τ in UNSB leads to unstable training. Hence, we believe adapting UNSB to high τ for multi-modal translation is also an interesting research direction.

Societal impacts. UNSB extends diffusion to translation between two arbitrary distributions, allowing us to explore a wider range of applications. In particular, UNSB may be used in areas with beneficial impacts, such as medical image restoration. However, UNSB may also be used to create malicious content such as fake news, and this must be prevented through proper regulation.

Reproducibility. We upload a file containing the code for our main experiments as a supplementary material. Furthermore, pseudo-codes and hyper-parameters are described in the main paper and the Appendix.

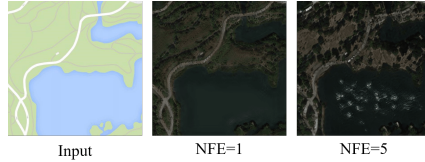


Figure 8: Example of a failure case. Occasional over-translation may occur with more NFEs, leading to artifacts.

7 Conclusion

In this work, we proposed Unpaired Neural Schrödinger Bridge (UNSB) which solves the Schrödinger Bridge problem (SBP) via adversarial learning. The adversarial learning formulation of SBP allowed us to combine SB with GAN training techniques for unpaired image-to-image translation. We demonstrated the scalability and effectiveness of UNSB through various data-to-data or image-to-image translation tasks. In particular, while all previous methods for SB or OT fail, UNSB achieved results that often surpass those of one-step models. Overall, our work opens up a previously unexplored research direction for applying diffusion models to unpaired image translation.

References

- [1] Jascha Sohl-Dickstein, Eric A. Weiss, Niru Maheswaranathan, and Surya Ganguli. Deep unsupervised learning using nonequilibrium thermodynamics. In *ICML*, 2015.
- [2] Jonathan Ho, Ajay Jain, and Pieter Abbeel. Denoising diffusion probabilistic models. In *NeurIPS*, 2020.
- [3] Jiaming Song, Chenlin Meng, and Stefano Ermon. Denoising diffusion implicit models. In *ICLR*, 2021.
- [4] Yang Song, Jascha Sohl-Dickstein, Diederik P. Kingma, Abhishek Kumar, Stefano Ermon, and Ben Poole. Score-based generative modeling through stochastic differential equations. In *ICLR*, 2021.
- [5] Zhisheng Xiao, Karsten Kreis, and Arash Vahdat. Tackling the generative learning trilemma with denoising diffusion gans. In *ICLR*, 2022.
- [6] Ian Goodfellow, Jean Pouget-Abadie, Mehdi Mirza, Bing Xu, David Warde-Farley, Sherjil Ozair, Aaron Courville, and Yoshua Bengio. Generative adversarial nets. In *NeurIPS*, 2014.
- [7] Diederik P. Kingma and Max Welling. Auto-encoding variational bayes. In *ICLR*, 2014.
- [8] Laurent Dinh, David Krueger, and Yoshua Bengio. Nice: Non-linear independent components estimation. *arxiv preprint arXiv:1410.8516*, 2015.
- [9] Hyungjin Chung, Jeongsol Kim, Michael Thompson Mccann, Marc Louis Klasky, and Jong Chul Ye. Diffusion posterior sampling for general noisy inverse problems. In *ICLR*, 2023.
- [10] Robin Rombach, Andreas Blattmann, Dominik Lorenz, Patrick Esser, and Björn Ommer. High-resolution image synthesis with latent diffusion models. In *CVPR*, 2022.
- [11] Valentin De Bortoli, James Thornton, Jeremy Heng, and Arnaud Doucet. Diffusion schrödinger bridge with applications to score-based generative modeling. In *NeurIPS*, 2021.
- [12] Tianrong Chen, Guan-Hong Liu, and Evangelos Theodorou. Likelihood training of schrödinger bridge using forward-backward sdes theory. In *ICLR*, 2022.
- [13] Alexander Tong, Nikolay Malkin, Guillaume Huguette, Yanlei Zhang, Jarrod Rector-Brooks, Kilian Fatras, Guy Wolf, and Yoshua Bengio. Conditional flow matching: Simulation-free dynamic optimal transport. *arxiv preprint arXiv:2302.00482*, 2023.
- [14] Gefei Wang, Yuling Jiao, Qian Xu, Yang Wang, and Can Yang. Deep generative learning via schrödinger bridge. In *International Conference on Machine Learning*, pages 10794–10804. PMLR, 2021.
- [15] Guan-Hong Liu, Arash Vahdat, De-An Huang, Evangelos A. Theodorou, Weili Nie, and Anima Anandkumar. I2sb: Image-to-image schrödinger bridge. *arxiv preprint arXiv:2302.05872*, 2023.
- [16] Mauricio Delbracio and Peyman Milanfar. Inversion by direct iteration: An alternative to denoising diffusion for image restoration. *arxiv preprint arXiv:2303.11435*, 2023.
- [17] Xuan Su, Jiaming Song, Chenlin Meng, and Stefano Ermon. Dual diffusion implicit bridges for image-to-image translation. In *ICLR*, 2023.
- [18] Erwin Schrödinger. Sur la théorie relativiste de l’électron et l’interprétation de la mécanique quantique. *Annales de l’institut Henri Poincaré*, 2(4):269–310, 1932.
- [19] Christian Léonard. A survey of the schrödinger problem and some of its connections with optimal transport. *arxiv preprint arXiv:1308.0215*, 2013.
- [20] Kenneth F Caluya and Abhishek Halder. Reflected schrödinger bridge: Density control with path constraints. In *2021 American Control Conference (ACC)*, pages 1137–1142. IEEE, 2021.
- [21] Yongxin Chen, Tryphon T Georgiou, and Michele Pavon. Stochastic control liaisons: Richard sinkhorn meets gaspard monge on a schrodinger bridge. *Siam Review*, 63(2):249–313, 2021.
- [22] Francisco Vargas, Pierre Thodoroff, Austen Lamacraft, and Neil Lawrence. Solving schrödinger bridges via maximum likelihood. *Entropy*, 23(9):1134, 2021.
- [23] Yuyang Shi, Valentin De Bortoli, George Deligiannidis, and Arnaud Doucet. Conditional simulation using diffusion schrödinger bridges. In *Uncertainty in Artificial Intelligence*, pages 1792–1802. PMLR, 2022.
- [24] Guan-Hong Liu, Tianrong Chen, Oswin So, and Evangelos A Theodorou. Deep generalized schrödinger bridge. *arXiv preprint arXiv:2209.09893*, 2022.
- [25] Ella Tamir, Martin Trapp, and Arno Solin. Transport with support: Data-conditional diffusion bridges. *arXiv preprint arXiv:2301.13636*, 2023.
- [26] James Thornton, Michael Hutchinson, Emile Mathieu, Valentin De Bortoli, Yee Whye Teh, and Arnaud Doucet. Riemannian diffusion schrödinger bridge. *arXiv preprint arXiv:2207.03024*, 2022.
- [27] Qinsheng Zhang and Yongxin Chen. Path integral sampler: a stochastic control approach for sampling. *arXiv preprint arXiv:2111.15141*, 2021.

- [28] Hamza Ruzayqat, Alexandros Beskos, Dan Crisan, Ajay Jasra, and Nikolas Kantas. Unbiased estimation using a class of diffusion processes. *Journal of Computational Physics*, 472:111643, 2023.
- [29] Phillip Isola, Jun-Yan Zhu, Tinghui Zhou, and Alexei A Efros. Image-to-image translation with conditional adversarial networks. In *Proceedings of the IEEE conference on computer vision and pattern recognition*, pages 1125–1134, 2017.
- [30] Jun-Yan Zhu, Taesung Park, Phillip Isola, and Alexei A. Efros. Unpaired image-to-image translation using cycle-consistent adversarial networks. In *Proceedings of the IEEE International Conference on Computer Vision (ICCV)*, Oct 2017.
- [31] Xun Huang, Ming-Yu Liu, Serge Belongie, and Jan Kautz. Multimodal unsupervised image-to-image translation. In *Proceedings of the European Conference on Computer Vision (ECCV)*, September 2018.
- [32] Huan Fu, Mingming Gong, Chaohui Wang, Kayhan Batmanghelich, Kun Zhang, and Dacheng Tao. Geometry-consistent generative adversarial networks for one-sided unsupervised domain mapping. In *Proceedings of the IEEE/CVF Conference on Computer Vision and Pattern Recognition (CVPR)*, June 2019.
- [33] Sagie Benaim and Lior Wolf. One-sided unsupervised domain mapping. In I. Guyon, U. V. Luxburg, S. Bengio, H. Wallach, R. Fergus, S. Vishwanathan, and R. Garnett, editors, *Advances in Neural Information Processing Systems*, volume 30. Curran Associates, Inc., 2017.
- [34] Taesung Park, Alexei A. Efros, Richard Zhang, and Jun-Yan Zhu. Contrastive learning for unpaired image-to-image translation. In Andrea Vedaldi, Horst Bischof, Thomas Brox, and Jan-Michael Frahm, editors, *Computer Vision – ECCV 2020*, pages 319–345, Cham, 2020. Springer International Publishing.
- [35] Chanyong Jung, Gihyun Kwon, and Jong Chul Ye. Exploring patch-wise semantic relation for contrastive learning in image-to-image translation tasks. In *Proceedings of the IEEE/CVF Conference on Computer Vision and Pattern Recognition (CVPR)*, pages 18260–18269, June 2022.
- [36] Weilun Wang, Wengang Zhou, Jianmin Bao, Dong Chen, and Houqiang Li. Instance-wise hard negative example generation for contrastive learning in unpaired image-to-image translation. In *Proceedings of the IEEE/CVF International Conference on Computer Vision (ICCV)*, pages 14020–14029, October 2021.
- [37] Chuanxia Zheng, Tat-Jen Cham, and Jianfei Cai. The spatially-correlative loss for various image translation tasks. In *Proceedings of the IEEE/CVF Conference on Computer Vision and Pattern Recognition (CVPR)*, pages 16407–16417, June 2021.
- [38] Paolo Dai Pra. A stochastic control approach to reciprocal diffusion processes. *Applied Mathematics and Optimization*, 23(1):313–329, 1991.
- [39] Aram-Alexandre Pooladian, Heli Ben-Hamu, Carles Domingo-Enrich, Brandon Amos, Yaron Lipman, and Ricky T. Q. Chen. Multisample flow matching: Straightening flows with minibatch couplings. In *ICML*, 2023.
- [40] Alexander Korotin, Daniil Selikhanovych, and Evgeny Burnaev. Neural optimal transport. In *ICLR*, 2023.
- [41] Martin Heusel, Hubert Ramsauer, Thomas Unterthiner, Bernhard Nessler, and Sepp Hochreiter. Gans trained by a two time-scale update rule converge to a local nash equilibrium. *Advances in neural information processing systems*, 30, 2017.
- [42] Runfa Chen, Wenbing Huang, Binghui Huang, Fuchun Sun, and Bin Fang. Reusing discriminators for encoding: Towards unsupervised image-to-image translation. In *Proceedings of the IEEE/CVF conference on computer vision and pattern recognition*, pages 8168–8177, 2020.
- [43] Mohamed Ishmael Belghazi, Aristide Baratin, Sai Rajeswar, Sherjil Ozair, Yoshua Bengio, Aaron Courville, and R Devon Hjelm. Mutual information neural estimation. In *ICML*, 2018.
- [44] Jae Hyun Lim, Aaron Courville, Christopher Pal, and Chin-Wei Huang. Ar-dae: Towards unbiased neural entropy estimation. In *ICML*, 2020.

A Proofs

Theorem 1 (Self-similarity) *Let $[t_a, t_b] \subseteq [0, 1]$ and $\{\mathbf{x}_t\} \sim \mathbb{Q}^{\text{SB}}$. The SB restricted to $[t_a, t_b]$, defined as the distribution of $\{\mathbf{x}_t\}|_{[t_a, t_b]} := \{\mathbf{x}_{t(s)} : s \in [0, 1]\}$ where $t(s) := t_a + (t_b - t_a)s$ solves*

$$\min_{\mathbb{Q} \in \mathcal{P}(\Omega)} D_{\text{KL}}(\mathbb{Q} \| \mathbb{W}^{\tau(t_b - t_a)}) \quad \text{s.t.} \quad \mathbb{Q}_0 = \mathbb{Q}_{t_a}^{\text{SB}}, \quad \mathbb{Q}_1 = \mathbb{Q}_{t_b}^{\text{SB}}. \quad (17)$$

Proof. We claim \mathbf{u}_t^{SB} restricted to the interval $[t_a, t_b]$ is also a SB from $\mathbb{Q}_{t_a}^{\text{SB}}$ to $\mathbb{Q}_{t_b}^{\text{SB}}$. Suppose the claim is false, so there is another drift $\hat{\mathbf{u}}_t$ on $[t_a, t_b]$ such that

$$\mathbb{E} \left[\int_{t_a}^{t_b} \|\hat{\mathbf{u}}_t\|^2 dt \right] < \mathbb{E} \left[\int_{t_a}^{t_b} \|\mathbf{u}_t^{\text{SB}}\|^2 dt \right] \quad \text{and} \quad \begin{cases} d\mathbf{x}_t = \hat{\mathbf{u}}_t dt + \sqrt{\tau} d\mathbf{w}_t, \\ \mathbf{x}_{t_a} \sim \mathbb{Q}_{t_a}^{\text{SB}}, \quad \mathbf{x}_{t_b} \sim \mathbb{Q}_{t_b}^{\text{SB}}. \end{cases}$$

We can extend $\hat{\mathbf{u}}_t$ to the entire interval $[0, 1]$ by defining

$$\hat{\mathbf{u}}_t = \begin{cases} \mathbf{u}_t^{\text{SB}} & \text{if } 0 \leq t < t_a, \\ \hat{\mathbf{u}}_t & \text{if } t_a \leq t < t_b, \\ \mathbf{u}_t^{\text{SB}} & \text{if } t_b \leq t < 1. \end{cases}$$

We then have

$$\mathbb{E} \left[\int_0^1 \|\hat{\mathbf{u}}_t\|^2 dt \right] < \mathbb{E} \left[\int_0^1 \|\mathbf{u}_t^{\text{SB}}\|^2 dt \right] \quad \text{and} \quad \begin{cases} d\mathbf{x}_t = \hat{\mathbf{u}}_t dt + \sqrt{\tau} d\mathbf{w}_t, \\ \mathbf{x}_0 \sim \pi_0, \quad \mathbf{x}_1 \sim \pi_1, \end{cases}$$

which contradicts our assumption that \mathbf{u}_t^{SB} solves Eq. (3). Finally, we note that by time scaling,

$$d\mathbf{x}_t = \mathbf{u}_t^{\text{SB}} dt + \sqrt{\tau} d\mathbf{w}_t, \quad t_a \leq t \leq t_b$$

is equivalent to the SDE

$$d\mathbf{x}_t = (t_b - t_a) \mathbf{u}_{s(t)}^{\text{SB}} dt + (t_b - t_a) \sqrt{\tau} d\mathbf{w}_{s(t)}, \quad 0 \leq t \leq 1$$

By the definition of the white noise process¹, $\mathbf{w}_{s(t)}$ is also a white noise process. It follows that we may replace $\mathbf{w}_{s(t)}$ with \mathbf{w}_t to obtain an equivalent SDE

$$d\mathbf{x}_t = (t_b - t_a) \mathbf{u}_{s(t)}^{\text{SB}} dt + (t_b - t_a) \sqrt{\tau} d\mathbf{w}_t, \quad 0 \leq t \leq 1$$

By comparing the stochastic control formulation Eq. (3) with the original SBP Eq. (1), we see that this means the reference Wiener measure for the SBP restricted to $[t_a, t_b]$ has variance $(t_b - t_a)\tau$. \square

Corollary 1.1 (CFM formulation of restricted SBs) *Let $t \in [t_a, t_b] \subseteq [0, 1]$ and $\{\mathbf{x}_t\} \sim \mathbb{Q}^{\text{SB}}$. Then*

$$p(\mathbf{x}_t | \mathbf{x}_{t_a}, \mathbf{x}_{t_b}) = \mathcal{N}(\mathbf{x}_t | s(t)\mathbf{x}_{t_b} + (1 - s(t))\mathbf{x}_{t_a}, s(t)(1 - s(t))\tau(t_b - t_a)\mathbf{I}) \quad (18)$$

where $s(t) := (t - t_a)/(t_b - t_a)$ is the inverse function of $t(s)$. Moreover,

$$\mathbb{Q}_{t_a t_b}^{\text{SB}} = \arg \min_{\gamma \in \Pi(\mathbb{Q}_{t_a}, \mathbb{Q}_{t_b})} \mathbb{E}_{(\mathbf{x}_{t_a}, \mathbf{x}_{t_b}) \sim \gamma} [\|\mathbf{x}_{t_a} - \mathbf{x}_{t_b}\|^2] - 2\tau(t_b - t_a)H(\gamma). \quad (19)$$

Proof. Translate the SBP Eq. (17) into the CFM formulation, taking into account the reduced variance $\tau(t_b - t_a)$ of the reference Wiener measure $\mathbb{W}^{\tau(t_b - t_a)}$. \square

B Omitted Experiment Details

To incorporate the timestep embedding and stochastic conditioning, we re-implemented the normalization layer of model as adaptive form. For timestep embedding, we use positional embedding with following the implementation of DDGAN [5]. For injecting stochastic condition, we use adaptive instance normalization layer. All of the experiments are conducted using single RTX3090 GPU. For loss functions, we used adversarial loss D_{KL} as identical loss proposed in CUT. To estimate the entropy loss, we used neural entropy estimation methods [43, 44]. For hyperparameters of the Schrödinger loss \mathcal{L}_{SB} , we used $\lambda_{SB} = 1$ and $\tau = 0.01$.

For feature selection of patch-wise contrastive learning loss in our \mathcal{L}_{Reg} , we used the same feature selection protocol in CUT. In the experiments on Summer \rightarrow Winter, we used pre-trained VGG16 network as our feature selection source, following the strategy in the previous work [37].

¹ \mathbf{w}_t and $\mathbf{w}_{t'}$ are independent if $t \neq t'$, and the mapping $t \mapsto \mathbf{w}_t$ is a Gaussian process with zero mean and Dirac delta correlation.

Method	H→Z	
	FID ↓	KID↓
SBCFM	229.5	18.8
Ours	35.7	0.587

Table 3: Quantitative comparison result with another SB-based method. The baseline model performance is severely degraded, while our generated results show superior perceptual quality. H→Z: Horse→Zebra.

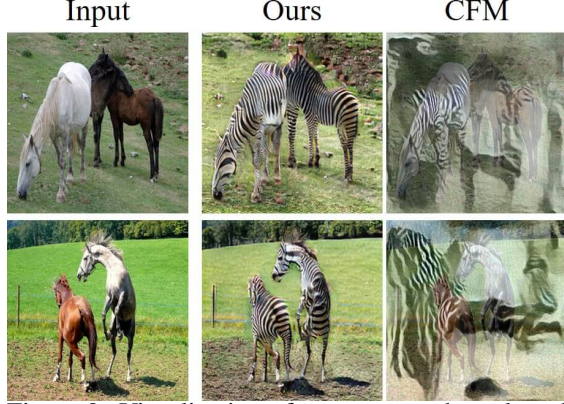


Figure 9: Visualization of our generated result and the result from conditional flow matching (CFM).

C Additional Experiments

C.1 Other SB Methods

In this part, we compare our proposed UNSB with other Schrödinger bridge based image translation methods. The recent work of I^2 SB and InDI require supervised training setting, therefore we cannot compare our proposed method with the baselines. For most of other SB-based methods, they focus on relatively easy problem, where one side of distribution is simple. Since we firstly proposed applying SB-based approach to high-resolution I2I problem, there is no direct baseline to compare. However, we compared our model with SB-based approach of Schrödinger Bridge Conditional Flow Matching (SB-CFM) [23] by adapting the SB-CFM to high-resolution case.

In Table 3 and Fig. 9, we can see that the baseline SB-CFM model could not generate the proper outputs where the outputs are totally unrelated to the input image. The results show that the model could not overcome the curse of dimensionality problem.

D Additional Samples

In Fig. 10, 11, we show additional generated samples from our proposed UNSB and baseline models.

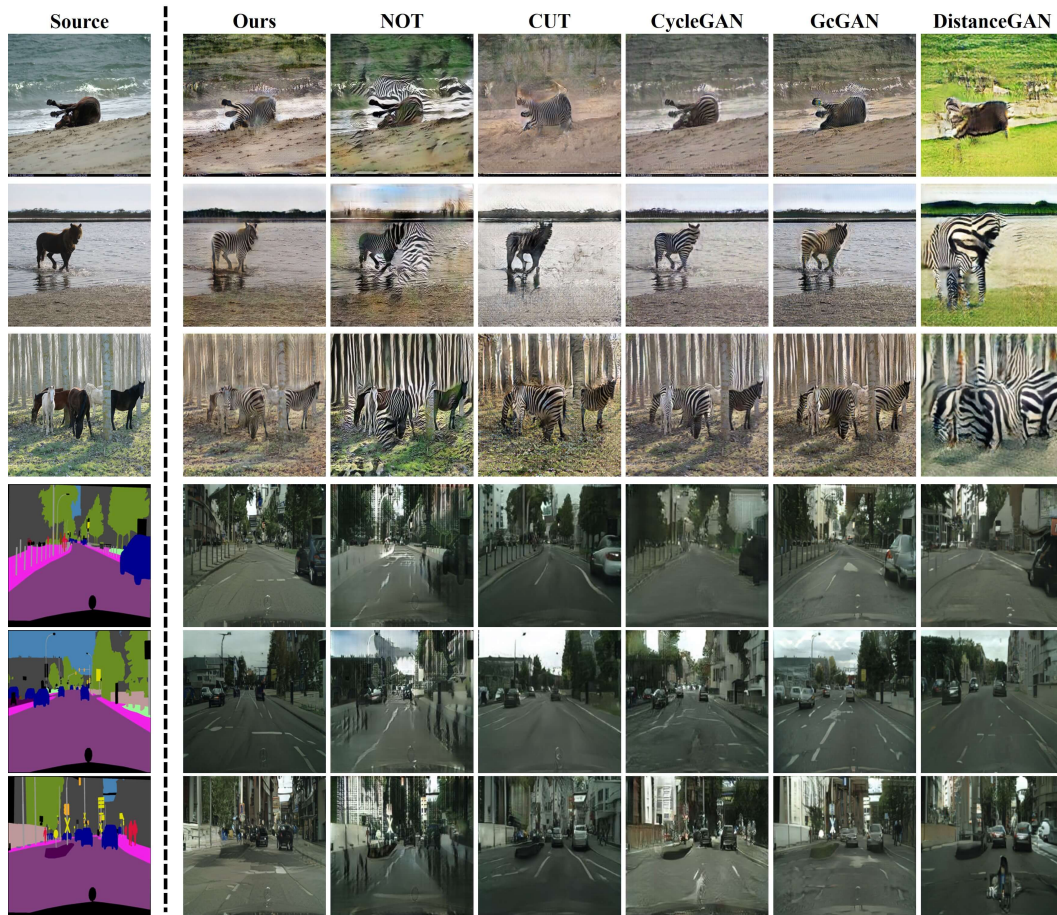


Figure 10: Additional samples from ours and baseline models of Horse→Zebra and Label→Cityscapes dataset.

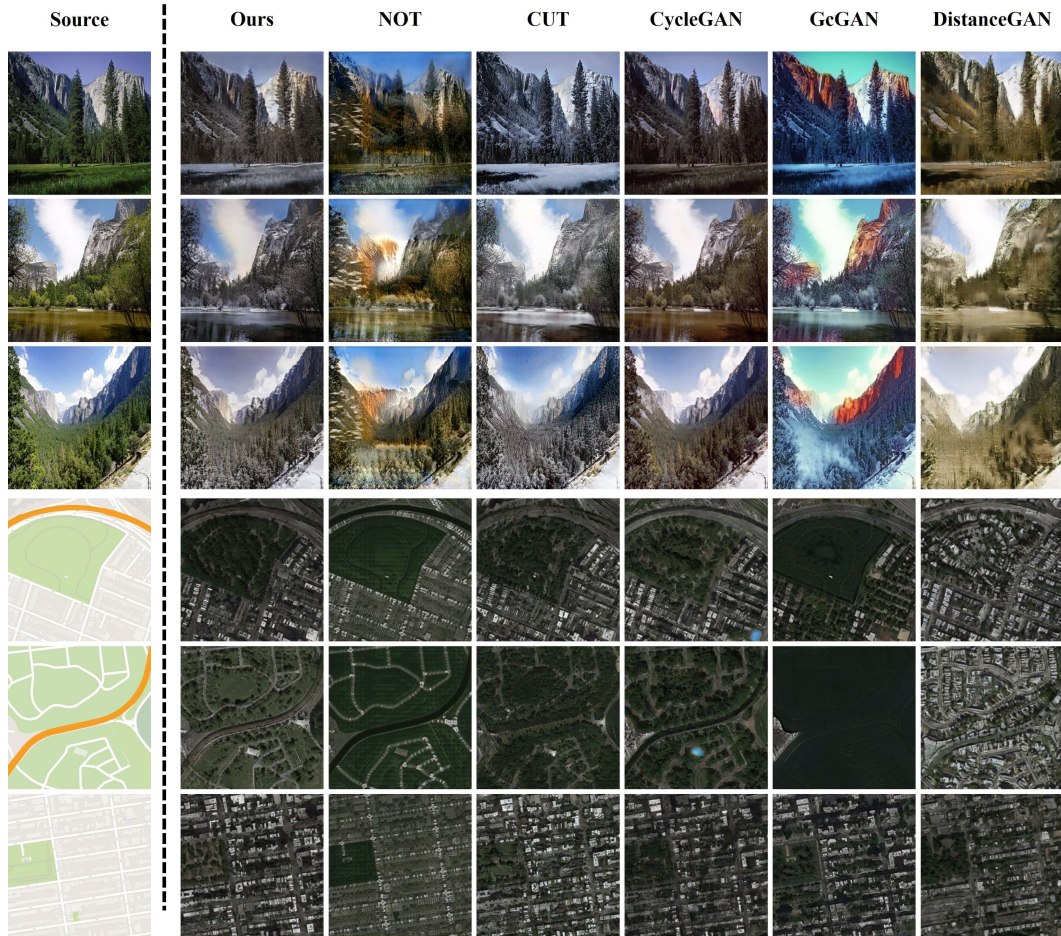


Figure 11: Additional samples from ours and baseline models of Summer→Winter and Map→Satellite dataset.